Bicycle Flow Dynamics of Cyclist Loading and Unloading Processes at Bottlenecks

Ning Guo[1], Wai Wong[2], Rui Jiang[3,*], S. C. Wong[4,5,*], Qing-Yi Hao[6], Chao-Yun Wu[6]

[1]*School of Automotive and Transportation Engineering, Hefei University of Technology, 230009, Hefei, P.R. China*

[2] *Department of Civil and Natural Resources Engineering, University of Canterbury, Christchurch, New Zealand*

[3] *School of Systems Science, Beijing Jiaotong University, 100044, Beijing, P.R. China*

[4] *Department of Civil Engineering, The University of Hong Kong, Pokfulam Road, Hong Kong, P.R. China*

[5] *Guangdong - Hong Kong - Macau Joint Laboratory for Smart Cities*

[6] *School of Mathematics and Computational Science, Anqing Normal University, 246133, Anqing, P.R. China*

Abstract

Cycling has emerged as one of the most important green transport modes in recent years, with cities increasingly prioritizing cycling in their sustainable policy agenda. However, the associated traffic dynamics, especially the evolution of bicycle flow at bottlenecks, have not been extensively studied. In this study, real-world experiments were conducted to investigate the dynamics of bicycle flow at bottlenecks under varying cycling demands generated by the cyclist unloading and loading processes. Upon the activation of the bottleneck, its capacity remained largely constant. For the same physical system, the bottleneck capacity of the cyclist loading process exceeded that of the unloading process, indicating the occurrence of capacity drop and hysteresis. Statistical analyses demonstrated that the capacity drop was attributable to the difference in speeds of the two processes for the same cycling

[*] Corresponding authors, Email: jiangrui@bjtu.edu.cn, hhecwsc@hku.hk.

demands after the bottleneck activation. These findings could potentially be explained by behavioral inertia. Further analysis revealed that compared with the unloading process, the cyclist loading process was associated with higher cycling speeds owing to the higher overtaking rates. The outcomes of this study can advance our understanding of the physics of bicycle flow dynamics and provide valuable insights for transport planning professionals involved in the facility planning and control of existing networks.

Keywords: bicycle flow dynamics; bottleneck capacity; capacity drop; hysteresis; behavioral inertia

1. Introduction

In recent years, urban regions have placed increasing emphasis on promoting cycling as a sustainable transport mode through the continuous planning and improvement of bicycle facilities and the expansion of bicycle networks (Olmos et al., 2020; Barrero and Rodriguez-Valencia, 2022). Given the growing importance of bicycles in urban transport, it is necessary to understand bicycle flow dynamics. The underlying physics and traffic flow theory can help to optimize system efficiency and can inform the development of rational infrastructure planning, network design, and management strategies.

Bottlenecks are key topics in the study of traffic flows, as they can cause interruptions in a traffic stream, resulting in congestion upstream and free flow downstream. Bottlenecks can be categorized as long term or short term. Long-term bottlenecks, such as lane drops and merging lanes, are typically stationary and result from physical constraints or operational requirements. Short-term bottlenecks are formed temporarily due to random events and can be either stationary, such as partial blockages at

incident sites, or mobile, such as a slow-moving platoon of vehicles. Bottlenecks can be found in vehicular flows (Meng and Weng, 2011; Jin and Jin, 2015), pedestrian streams (Hoogendoorn and Daamen, 2005; Seyfried et al., 2009), and bicycle traffic. Given the prevalence of bottlenecks in cycle tracks, it is necessary to clarify the bicycle flow dynamics at such sites to facilitate effective infrastructure planning, traffic management, and control.

Despite the importance of bottlenecks in traffic flow theory, studies on bicycle flow have typically focused on aspects such as bicycle flow capacity (Homburger, 1976; Botma and Papendrecht, 1991; Raksuntorn and Khan, 2003), service quality (Beura et al., 2017), fundamental diagrams (Navin, 1994), and cyclist behaviors (Paulsen et al., 2019). Bicycle flow capacities for different locations worldwide have been identified. For example, in Davis, California, a 1-m-wide cycle track has a bicycle flow capacity of approximately 2600 cyclists/h/m (Homburger, 1976), whereas a study in the Netherlands observed a capacity of 3850 to 4480 cyclists/h/m for a 0.78-m-wide cycle track (Botma and Papendrecht, 1991). Additionally, Raksuntorn and Khan (2003) determined the maximum bicycle flow rate at the stop line of signalized intersections to be 1875 cyclists/h/m for a 0.78-m-wide cycle track. By examining the quantitative factors influencing the service quality for cyclists, Beura et al. (2017) investigated bicycle movements at signalized intersections. Additionally, fundamental diagrams have been used to depict bicycle flow dynamics. Navin (1994) conducted a controlled experiment involving a group of teenagers riding behind a leader on a 4-m-wide and 125-m-long oval cycle track. The results revealed that a maximum bicycle flow of over 60 cyclists/min/m could be reached at a bicycle density of approximately 0.3 cyclists/m^2. Later, Mai et al. (2012) and Jiang et al. (2017) conducted single-file

bicycle flow experiments on a 146-m-long circular cycle track and an on-ramp system. These experiments yielded a unimodal fundamental diagram and found that traffic jams spontaneously form beyond a critical bicycle density of 0.37 cyclists/m. Similarly, Zhang et al. (2014) conducted a single-file bicycle flow experiment on an 86-m-long cycle track, and observed the transition from free flow to a congestion state at a density of approximately 0.3 cyclists/m and stop-and-go waves when the density reached 0.384 cyclists/m, which was consistent with the findings of Jiang et al. (2017). However, these single-file flow experiments do not fully capture real-world cycling scenarios in which cyclists may follow, ride side-by-side, or overtake one another. Therefore, Guo et al. (2021) conducted a series of bicycle flow experiments on a 3-m-wide cycle track. Unlike the reported unimodal model, a trapezoidal fundamental diagram was observed, with a nearly constant bicycle flow at the peak level over a wide range of densities. The researchers suggested that the formation of new bicycle lanes across the 3-m-wide cycle track potentially contributed to the delayed drop in the bicycle flow. In terms of cyclist behavior, Paulsen et al. (2019) observed a forced-following phenomenon, in which faster cyclists are impeded by slower ones even at moderate densities. By analyzing video footage from the Brooklyn Bridge in New York City, Mohammed et al. (2019) noted that factors such as the longitudinal distance, lateral distance, and speed difference likely influenced cyclists' decisions to follow or overtake. Gavriilidou et al. (2019), who conducted an experiment on a wide cycle track, found that many cyclists overtook on curves rather than on straight sections and preferred maintaining spacing by following at lower speeds rather than stopping.

Various models have been developed to represent bicycle flow dynamics. For example, Jiang et al. (2004) and Jia et al. (2007) proposed multi-value cellular automaton models based on stochastic randomization mechanisms to improve bicycle flow models. To account for the higher speed of electric bikes compared with conventional bikes, Jin et al. (2015) incorporated the maximum speed of electric bikes into a multi-value cellular automaton model. Using a following-move mechanism, Xue et al. (2017) developed an improved multi-value cellular model to accurately explain experimental and field data. Gould and Karner (2009) developed a lane-change cellular automaton model for bicycle flow. Ren et al. (2016) developed a cellular automata model that considers dispersion and found that the traffic efficiency could be improved in the case of increased spilling and overtaking maneuvers at intersections. Liang et al. (2012) incorporated social force and trajectory choice into a psychological–physical force model. Recently, Guo et al. (2020) extended a heuristic-based model to simulate the mixed flow of pedestrians and bicycles.

Although many researchers have focused on bicycle flow dynamics and developed associated models, the investigation of bicycle flows at bottlenecks has received limited attention. Ren et al. (2016) used a cellular automata model to study how the area occupied by bicycles at an intersection expands and contracts. Paulsen et al. (2019) investigated a lane-drop case using a speed-heterogeneity lane-choice model and found that the delay was concentrated around the bottleneck. Moreover, several studies have reported that the bottleneck capacity depends on the local density. Wierbos et al. (2021) investigated the influence of the local bicycle density immediately upstream of a bottleneck on the bottleneck capacity at controlled intersections, which are common bottlenecks for cyclists. The results

indicated that the bottleneck capacity increases with increasing local density owing to the empty space downstream of the bottleneck, and the discharge rate varies with the queue configuration. Wierbos et al. (2019) confirmed the positive correlation between the bottleneck capacity and bottleneck width by conducting cycling experiments involving 34 cyclists, constituting a fixed demand, and different bottleneck widths. The results showed that the bottleneck capacity increases linearly with the bottleneck width for values ranging between 0.5 m and 1.5 m.

Notably, the bicycle flow demand is not constant in real-world scenarios and varies over time. During morning peak hours, cyclists from various residential areas converge toward the central business district (CBD), resulting in increasing bicycle flow demand. This process is referred to as the cyclist loading process. Conversely, during afternoon peak hours, cyclists disperse from the CBD to different destinations, leading to decreasing bicycle flow demand. This process corresponds to the cyclist unloading process. Capacity drop and hysteresis are commonly observed in vehicular flow, attributable to the traffic loading and unloading processes (Saberi and Mahmassani, 2013; Ni, 2021). At the same density, the flow during the unloading process is lower than that in the loading process. To the best of our knowledge, no studies have explored the bicycle flow dynamics at bottlenecks under varying demand. Thus, the underlying cycling behaviors, presence of capacity drop and hysteresis, and the impact of these phenomena on the bottleneck capacity remain unexplored. The capacity of a cycle track is a crucial parameter for its planning, design, and management. In the presence of capacity drop and hysteresis, the bottleneck capacity may be lower in certain demand conditions. This highlights the need for carefully considered and conservative estimates, such as the use of a lower bottleneck capacity, in

cycle track design to ensure optimal and efficient utilization of the infrastructure and urban spaces. With the growing significance of cycling in urban transportation systems, it is necessary to investigate the bicycle flow dynamics at bottlenecks under varying demands.

To fill this research gap, a series of comprehensive experiments on cycle track operations were conducted to investigate the bicycle flow dynamics at bottlenecks under varying demand. Two demand patterns were considered: (1) decreasing demand, corresponding to cyclist unloading, and (2) increasing demand, corresponding to cyclist loading. The results showed that the bottleneck capacity during the cyclist loading process was greater than that during the cyclist unloading process, indicating the presence of capacity drop and hysteresis. These phenomena could be attributed to the significant differences in speeds between the two processes, resulting from the cyclists' behavioral inertia, i.e., their tendency to maintain their previous riding behavior. Further analysis indicated that the higher speeds observed during the cyclist loading process relative to the speeds in the unloading process correlated with higher overtaking rates among cyclists.

The remainder of this paper is organized as follows. Sections 2 and 3 describe the experimental design and setup, respectively. Sections 4 and 5 describe the data extraction and constitution processes, respectively. Section 6 discusses the results of data analysis. Section 7 presents the concluding remarks.

2. Experimental Design

2.1. Objective

The objective of this study was to design and conduct a series of comprehensive experiments investigating the presence of capacity drop and hysteresis in the cyclist unloading and loading processes and, if these phenomena existed, to explore the potential contributing factors.

2.2. Cycle track design

The ideal experimental design to study bicycle flow dynamics at bottlenecks would involve a straight cycle track with a bottleneck to eliminate the potential influence of geometrical factors on cycling behavior. However, due to the practical challenges of recruiting a large number of participants for an extended period, a classic oval-shaped cycle track, allowing multiple rounds of cycling, has been typically used for this type of research.

In such settings, the choices of the track layout, including the lengths of straight segments and radii of the semi-circular segments at the two ends of the cycle track, are crucial. The radii of the semi-circular segments should be sufficiently large to minimize the impact on speed profiles due to turning, and the straight segments must be adequately large to allow cyclists to return to their desired speed before approaching the bottleneck. Nonetheless, it is important to balance these parameters to avoid cycling fatigue and prolonged experimental periods.

2.2.1 Single-cyclist experiment to examine the speed profile evolution

A series of single-cyclist experiments were conducted to determine a suitable combination of the abovementioned parameters. The objective was to examine the evolution of speed profiles for cyclists on different cycle tracks with varying radii at the two ends. To ensure that any changes in speed profiles

were solely due to the track geometry and not cyclist-to-cyclist interactions, only one cyclist was involved in each experimental run.

This single-cyclist experiment was conducted on September 10, 2022, at Hefei University of Technology, China. Four oval-shaped cycle tracks were established, as depicted in Figure 1.

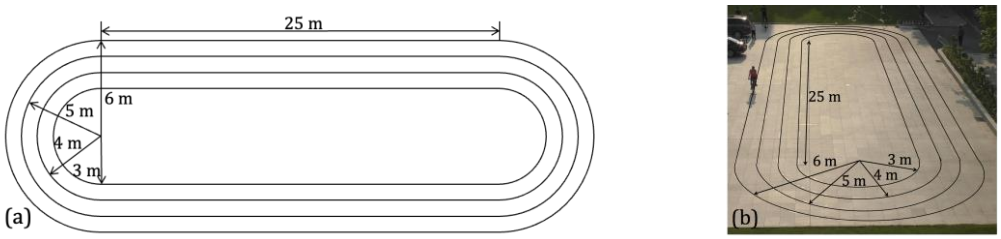

Figure 1. Single-cyclist experiment to study the speed profile evolution: (a) schematic of the cycle tracks with radii of 3 m, 4 m, 5 m, and 6 m; and (b) snapshot of the single-cyclist experiment conducted on the 6-m radius track.

The radii of the semi-circular segments of each track were set as 3 m, 4 m, 5 m, and 6 m, and the length of the straight segments was set as 25 m. Ten undergraduate students, seven male and three female, participated in the experiment. The cyclists were instructed to ride on the track as they normally would, without being informed of the experiment's objective. Each participant was instructed to first ride on the cycle track in an anticlockwise direction, starting with four laps on the 6-m radius track, followed by four laps on the 5-m radius track, four laps on the 4-m radius track, and four laps on the 3-m radius track. The same sequence was then repeated in the clockwise direction.

2.2.2 Data extraction

The experiment was recorded using a Panasonic HC-VX980 video camera, operating at a frame rate of 50 frames per second. The camera was positioned on the highest floor of a building adjacent to the cycle track, 25 m horizontally and 16 m vertically from the center of the cycle track. The tilt angle perpendicular to the camera was 58°, and the heights of the cyclists ranged from approximately 172 to

178 cm. The cyclists' trajectory data were extracted from the footage for every frame using PeTrack (Boltes et al., 2010). The maximum error of the projected location of a cyclist was approximately 6.3 cm. The speed profiles of the cyclists were obtained by analyzing the collected trajectory data.

2.2.3 Experimental results

To analyze the speed profiles, each lap was divided into two parts, each of which consisted of a semi-circular segment and a straight segment. Figure 2 shows the average speed profiles of the 10 participants on both segments for cycle tracks with different radii. The start point of the straight segment was set at 0 m. Negative values indicate the distance from the start of the straight segment back to the semi-circular segment. The starting points of the four average speed profiles shown in Figure 2 varied owing to differences in the lengths of the semi-circular segments among the four oval-shaped cycle tracks.

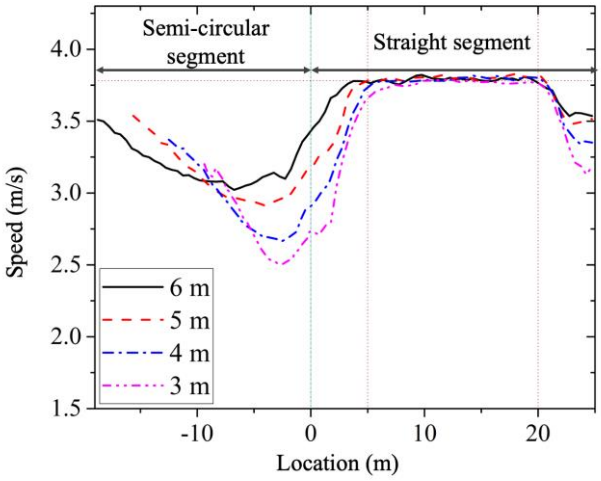

Figure 2. Average speed profiles of the 10 participants along the semi-circular segment and the straight segment for cycle tracks with different radii.

The speed profiles along the four cycle tracks exhibited consistent patterns. Upon entering the semi-circular segments, the participants decelerated. A smaller radius corresponded to a lower speed attained

by the cyclists. Before the participants exited the semi-circular segments, they began accelerating. Upon entering the straight segments, the participants continued to accelerate until they reached a common desired speed of about 3.8 m/s. All the participants achieved the desired speed within 5 m of entering the straight segment, except in the segments with a radius of 3 m, in which the attainment of the target speed took slightly longer. Before exiting the straight segments, the participants started decelerating approximately 5 m before entering the next semi-circular segment to prevent skidding.

2.2.4 Cycle track and bottleneck design

The results of the previous analysis suggested that in the case of the semi-circular segments with radii greater than 3 m, the effect of the segment on the speed profiles diminished after the initial 5 m and before the final 5 m of the straight segments. Thus, an oval-shaped cycle track (Figure 3), consisting of straight segments with a length of 25 m and semi-circular segments with inner and outer radii of 4 m and 7 m, respectively, was chosen. The width of the cycle track, w_c, was set as 3 m. A funnel-shaped bottleneck, with a length, entry width, and exit width w_b of 2 m, 3 m, and 1.5 m, respectively, was constructed using boxes. The exit of the bottleneck was positioned 5 m upstream of the semi-circular segment. The boundaries of the cycle track were defined using adhesive tape, and it covered an area of 253.7 m^2.

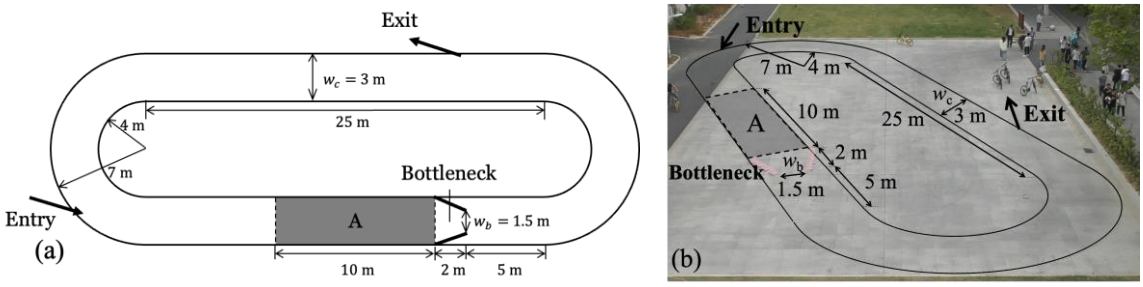

Figure 3. Cycle track with 1.5 m bottleneck: (a) schematic; and (b) real-world implementation.

2.3. Determination of the number of required participants

As the bottleneck was positioned 5 m upstream of the semicircle, and the cyclists took 5 m to reach their desired speeds after entering the straight segment, the maximum area available for "normal" cycling was 15 m in the middle of the straight segment. According to Wierbos (2021), the cycling jam density is approximately 0.7 cyclists/m^2, corresponding to 32 cyclists for a 15 m queue on the 3-m-wide track. To maintain a queue length of 15 m, the number of cyclists joining the tail of the queue should be the equal to the number leaving the queue through the bottleneck. The number of circulating cyclists depends on the bottleneck exit flow and cycling speed. The bottleneck exit flow of 1.82 cyclists/s pertaining to the 1.5-m-wide bottleneck considered by Wierbos (2021) was taken as the reference. According to the cycling speed in the single-cyclist experiment, approximately 23 s were required to ride from the bottleneck exit to the tail of the 15-m-long queue. Therefore, 42 cyclists (23 s × 1.82 cyclists/s) were additionally required, resulting in a total of 74 participants. To flexibly increase or decrease the number of participants in increments of 10, 80 participants were recruited.

2.4. Participant recruitment

Eighty undergraduate students, 54 men and 26 women, were recruited. Each participant was assigned a unique serial number ranging from 1 to 80. The purpose of the experiment was not disclosed to the participants, and they were instructed to cycle in a counterclockwise direction on the track in their normal manner.

2.5. Determination of the duration of each stage

To ensure that the experimental results were statistically significant, the duration of each stage, in which the number of cyclists was to be increased or decreased by 10, was required to be sufficient for participants to complete multiple cycles of the track and for the traffic conditions to reach a steady state. However, the duration of each stage could not be too long, as it would result in cycling fatigue. Following the approach used by Wierbos (2021), a duration that enabled the completion of 10 laps in free-flow conditions was selected. Based on the results of the single-cyclist experiment, in which a lap took 27 s to complete, the duration for each stage was set as 4.5 min (i.e., $27\ \text{s} \times 10/60\ \text{s/min} = 4.5$ min).

2.6. Experimental procedures

Four experimental runs were performed (Runs 1 to 4), with a 10 min break between Runs 2 and 3 to prevent cycling fatigue. Table 1 lists the number of cyclists and the corresponding serial numbers in each run. To realistically simulate the varying cycling demand, cyclist unloading and loading processes were devised. The cyclist unloading process, representing the transition from congestion to free flow, was replicated by allowing a large number of cyclists onto the cycle track at the start, activating the bottleneck shortly thereafter, and gradually decreasing the number of cyclists sequentially until the bottleneck was deactivated. The cyclist loading process, representing the transition from free flow to congestion, was replicated by introducing a small number of cyclists onto the cycle track and then gradually increasing the number of cyclists sequentially until the bottleneck was activated.

Table 1. Settings of the four experimental runs with a 1.5 m bottleneck

Run 1				Run 3			
Stage	Number of cyclists	Serial number	Duration (s)	Stage	Number of cyclists	Serial number	Duration (s)

1	80	1–80	270	1	80	1–80	270
2	70	1–70	270	2	70	11–80	270
3	60	1–60	270	3	60	21–80	270
4	50	1–50	270	4	50	31–80	270
5	40	1–40	270	5	40	41–80	270
6	30	1–30	270	6	30	51–80	270
7	20	1–20	270	7	20	61–80	270
8	10	1–10	270	8	10	71–80	270
Run 2				Run 4			
Stage	Number of cyclists	Serial number	Duration (s)	Stage	Number of cyclists	Serial number	Duration (s)
1	10	71–80	270	1	10	1–10	270
2	20	61–80	270	2	20	1–20	270
3	30	51–80	270	3	30	1–30	270
4	40	41–80	270	4	40	1–40	270
5	50	31–80	270	5	50	1–50	270
6	60	21–80	270	6	60	1–60	270
7	70	11–80	270	7	70	1–70	270
8	80	1–80	270	8	80	1–80	270

Run 1 simulated the cyclist unloading process. In Stage 1 of Run 1, cyclists numbered 1 to 80 were instructed to enter the cycle track. The 4.5-min timekeeping was initiated once the cyclists entered the track. In Stage 2, 10 cyclists numbered 71 to 80 left the cycle track while the remaining cyclists continued cycling. Another set of 4.5-min timekeeping was initiated once the 10 cyclists left the track.

Run 1 was followed by Run 2, which represented the cyclist loading process. In Stage 1 of Run 2, 10 cyclists numbered 71 to 80 (the first group of cyclists leaving the cycle track in Run 1) were instructed to enter the track. This was followed by a 4.5-min timekeeping period. In Stage 2, cyclists numbered 61 to 70 entered the track while the existing cyclists continued cycling. Another 4.5-min timekeeping period began.

After the 10 min break, Runs 3 and 4 were executed in the same way as Runs 1 and 2, except that they involved different combinations of cyclists with different serial numbers, which helped eliminate the influence of the ordering and individual characteristics of the participants.

3. Experimentation

This section presents several snapshots of the experiments conducted on October 16, 2022, at Hefei University of Technology, China, to illustrate the implementation of the experiment in the initial stages and the cyclist loading and unloading processes.

Figure 4 displays the snapshots of Run 1: (a) corresponds to the beginning of Stage 1 with 80 cyclists, and (b) corresponds to the end of Stage 1 with 10 cyclists leaving the cycle track. Shortly after Stage 1 commenced, the bottleneck was activated due to the large number of cyclists and the resulting intense interactions among the cyclists upstream of the bottleneck. This activation led to the formation of a steady upstream bicycle queue that persisted throughout the 4.5-min duration. At the end of Stage 1, 10 cyclists (71–80) were instructed to leave the cycle track. Subsequently, Run 1 was implemented as described in Table 1. As the number of cyclists gradually decreased, the upstream bicycle queue dissipated and vanished. Once the bottleneck was deactivated, the bicycle state transitioned from congestion to free flow.

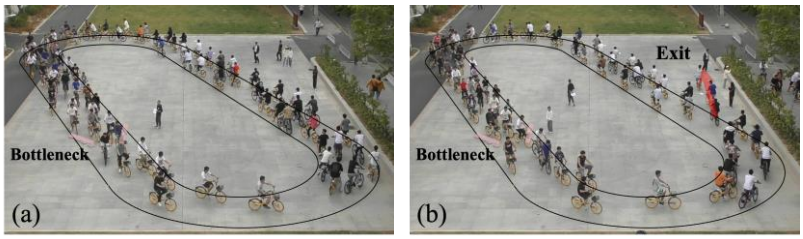

Figure 4. Run 1: (a) at the start of Stage 1 with 80 cyclists, and (b) at the end of Stage 1 with cyclists leaving the cycle track.

Figure 5 displays the snapshots of Run 2, with (a) corresponding to the start of Stage 1 with 10 cyclists and (b) corresponding to the end of Stage 1 with 10 cyclists entering the cycle track. In Stage 1, because only 10 cyclists were present on the cycle track, their interactions were minimal, and all of them could travel at their desired speeds. The bottleneck was not activated, and no upstream bicycle

queue was observed. After Stage 1, 10 cyclists (61–70) entered the cycle track. As the average bicycle density remained low, the interactions between cyclists were considered negligible. Subsequently, Run 2 was implemented as described in Table 1. As the number of cyclists gradually increased, the interactions among them increased, leading to the activation of the bottleneck and the transition of the bicycle state from free flow to congestion. As more cyclists joined, the length of the upstream bicycle queue gradually increased.

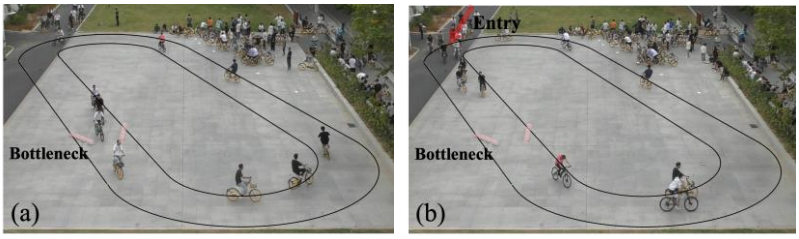

Figure 5. Run 2: (a) at the start of Stage 1 with 10 cyclists and (b) at the end of Stage 1 with cyclists entering the cycle track.

4. Data Extraction

The experiment was recorded using a Panasonic HC-VX980 video camera, operating at a frame rate of 50 frames per second. The camera was positioned on the highest floor of a building adjacent to the cycle track, at a horizontal distance of 11 m and a vertical distance of 24 m from the center of the track. The tilt angle perpendicular to the camera was 18°, and the heights of the participating cyclists ranged from approximately 160 to 180 cm. The cyclists' trajectories were extracted using PeTrack (Boltes et al., 2010). The maximum error of the projected location of a cyclist was approximately 4.3 cm. Furthermore, the extracted trajectories were verified using the Tracker software, as described in Appendix A.

5. Data Collection

5.1. Upstream subarea

To capture the bicycle flow dynamics through the bottleneck, an upstream subarea, marked as Area A in Figure 3, was chosen for measurement. The dimensions of the upstream subarea were selected to capture as much of the bicycle flow dynamics as possible while excluding the speed recovery region associated with the upstream semi-circular track. Therefore, the width of the upstream subarea was set as the full width of the cycle track, i.e., $w_c = 3$ m, and its length was set as 10 m, resulting in an area A of 30 m^2.

5.2. Density, speed, and flow analysis

Let $n(\tau)$ be the number of cyclists traveling in the upstream subarea at any time τ. The upstream bicycle density at time t, denoted as $k(t)$, $\forall t = 1, 2, 3, ...$, is

$$k(t) = \frac{\sum_{m=0}^{M-1} n(t - m\Delta\tau)}{MA}, \quad \text{Eq. (1)}$$

where m is the index representing the number of frames traced back from t, $\forall m \in [0, M-1]$. M is the number of frames in a second, set as 50 because the video was recorded at a rate of 50 frames per second. $\Delta\tau$ represents the time elapsed between two consecutive frames, equal to 0.02 s in this study.

Let $\vec{x}_i(\tau)$ to be the position vector of the i^{th} cyclist in the upstream area at any time τ. The upstream space-mean speed at time t, denoted as $u(t)$, is the total distance traveled by all cyclists in the upstream subarea during the time interval $[t-1, t]$ divided by the total time spent. This speed can be mathematically expressed as

$$u(t) = \frac{\sum_{m=0}^{M-1} \sum_{i=1}^{n(t-m\Delta\tau)} |\vec{x}_i(t - m\Delta\tau) - \vec{x}_i[t - (m+1)\Delta\tau]|}{\sum_{m=0}^{M-1} n(t - m\Delta\tau)\Delta\tau}. \quad \text{Eq. (2)}$$

The upstream bicycle flow across the cycle track at time t, denoted as $q(t)$, is the product of the cycle track width, w_c, upstream space-mean speed at time t, $u(t)$, and upstream bicycle density at time t, $k(t)$:

$$q(t) = w_c u(t) k(t). \quad \text{Eq. (3)}$$

5.3. Average density, average speed, and average flow analysis

Although the density, speed, and flow quantities in the previous subsection provide a detailed and high-resolution characterization of bicycle flow dynamics on a per-second basis, they may be susceptible to short-term noise resulting from stochasticity and randomness. To mitigate this effect, this subsection defines the average density, average speed, and average flow on a per-stage basis. This averaging approach effectively smooths out any noise present in the measurements and provides a more robust characterization of the underlying bicycle flow dynamics.

The average upstream bicycle density during stage T, $\forall T \in [1, 8]$, is given by

$$\bar{k}(T) = \frac{\sum_{h=0}^{H-1} n(TH - h\Delta\tau)}{HA}, \quad \text{Eq. (4)}$$

where h is the index representing the number of frames traced back from TH, $\forall h \in [0, H-1]$. H is the number of frames in a stage, set as 13,500 because the duration of a stage was 270 s ($H = 270 \times 50 = 13{,}500$).

The average upstream space-mean speed during stage T, denoted as $\bar{u}(T)$, is defined as the total distance traveled by all cyclists in the upstream subarea during stage T divided by the total time spent:

$$\bar{u}(T) = \frac{\sum_{h=0}^{H-1} \sum_{i=1}^{n(TH-h\Delta\tau)} |\vec{x}_i(TH - h\Delta\tau) - \vec{x}_i[TH - (h+1)\Delta\tau]|}{\sum_{h=0}^{H-1} n(TH - h\Delta\tau)\Delta\tau}. \quad \text{Eq. (5)}$$

The average upstream bicycle flow across the cycle track during stage T, denoted as $\bar{q}(T)$, is the product of the cycle track width, w_c; average upstream space-mean speed during stage T, $\bar{u}(T)$; and average upstream bicycle density during stage T, $\bar{k}(T)$:

$$\bar{q}(T) = w_c \bar{u}(T) \bar{k}(T). \quad \text{Eq. (6)}$$

6. Data Analysis And Results

6.1. Relationship between the average flow and average density

This subsection discusses the relationships between the average upstream bicycle flow and average upstream bicycle density. Figure 6 illustrates the relationship between $\bar{q}(T)$ and $\bar{k}(T)$ in (a) Runs 1 and 2 and (b) Runs 3 and 4 with the 1.5 m bottleneck. The unloading process, simulated by Run 1 in Figure 6a, could be divided into two parts by a critical density of approximately 0.125 cyclists/m^2. Beyond this critical density, the average upstream bicycle flow remained largely constant at approximately 1.15 cyclists/s, which was considered the bottleneck capacity for the cyclist unloading process. This constant average upstream bicycle flow indicated the activation of the bottleneck, which could be further confirmed by the snapshots of Stages 1–6 in Run 1, in which bicycle queues formed upstream of the bottleneck. Figure 7 shows the snapshots of the experiment with (a) 60 and (b) 40 cyclists in Run 1. As the number of cyclists decreased from 80 to 30, the average upstream bicycle density decreased. When the average upstream bicycle density decreased to a value below the critical density, the bottleneck was deactivated, and a free-flow state was established. Figure 8 displays the snapshots of the experiment with (a) 20 and (b) 10 cyclists, showing the absence of an upstream bicycle queue. The average upstream bicycle flow decreased approximately linearly with a decreasing average upstream bicycle density.

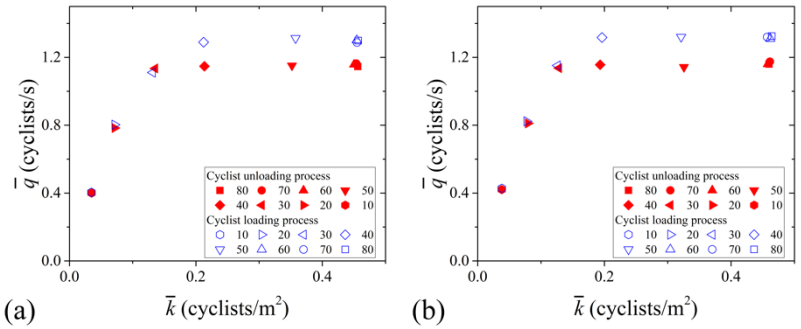

Figure 6. Relationship between $\bar{q}$ and $\bar{k}$ in (a) Runs 1 and 2 and (b) Runs 3 and 4 with the 1.5 m bottleneck.

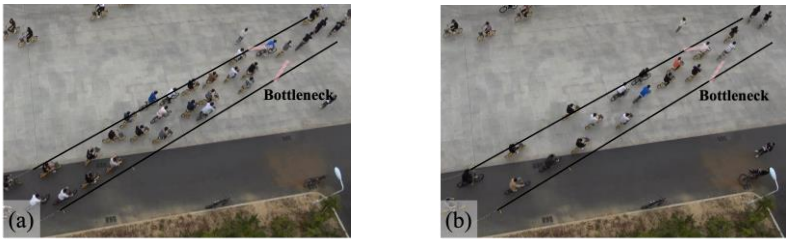

Figure 7. Snapshots of Run 1 experiment with (a) 60 and (b) 40 cyclists.

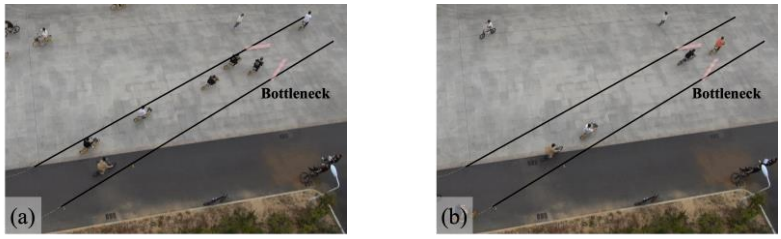

Figure 8. Snapshots of Run 1 experiment with (a) 20 and (b) 10 cyclists.

Run 2 was designed to simulate the cyclist loading process. This process could be divided into two parts by a critical density of approximately 0.2 cyclists/m^2. Below this critical density, the average upstream bicycle flow increased approximately linearly with an increasing average upstream bicycle density. When the average upstream bicycle density exceeded the critical density, the average upstream bicycle flow remained nearly constant at approximately 1.3 cyclists/s, which was considered the bottleneck capacity for the cyclist loading process. The constant average upstream bicycle indicated bottleneck activation, which could be verified by the footage of Run 2.

Interestingly, even when the same physical system was considered and the average upstream bicycle densities were identical, the bottleneck capacity of the cyclist loading process was higher than that of the cyclist unloading process. This observation indicated the occurrence of a capacity drop in response to varying cycling demands.

Figure 6b shows the results of Runs 3 and 4, which were similar to those of Runs 1 and 2, respectively. The ordering and individual characteristics of the cyclists did not significantly affect the results, and the observed capacity drop was noted to be a persistent pattern.

6.2. Density, speed, and flow evolutions

Although the per-stage analysis confirmed the occurrence of a capacity drop, the averaging effect obscured the bicycle flow dynamics and limited the investigation of its evolution at bottlenecks with varying cycling demands. To address this limitation, the high-resolution characterization of bicycle flow dynamics was realized on a per-second basis.

Figure 9 shows the evolution of k, u, and q over time for Runs 1 and 2 with the 1.5 m bottleneck. In Stage 1 of Run 1, when 80 cyclists gained access to the cycle track, k immediately increased to approximately 0.475 cyclists/m^2. Due to the intense interactions among cyclists, u was limited to a low value of approximately 0.8 m/s. As the number of cyclists decreased from 80 to 60, although some fluctuation was produced by the interactions between cyclists, k and u remained constant at approximately 0.475 cyclists/m^2 and 0.8 m/s, respectively. The constant nature and high value of k indicated that the upstream subarea was fully occupied by a bicycle queue. The upstream bicycle flow stabilized at a bottleneck capacity of approximately 1.15 cyclists/s. However, when the number of

cyclists further decreased from 60 to 30, k and u decreased and increased in a stepwise manner, respectively. These trends indicated that as the upstream bicycle queue dissipated, the cyclist density in the upstream subarea decreased, and these cyclists could accelerate. The stepwise patterns indicated that steady states could be reached within a few seconds after an unloading or loading process. The increasing and decreasing effects counterbalanced each other, and thus, q remained unchanged at the bottleneck capacity. As the number of cyclists decreased from 30 to 20 and 10, u continued to increase, but the effect of k decreasing outweighed the effect of this increase, leading to bottleneck deactivation and stepwise drops in q.

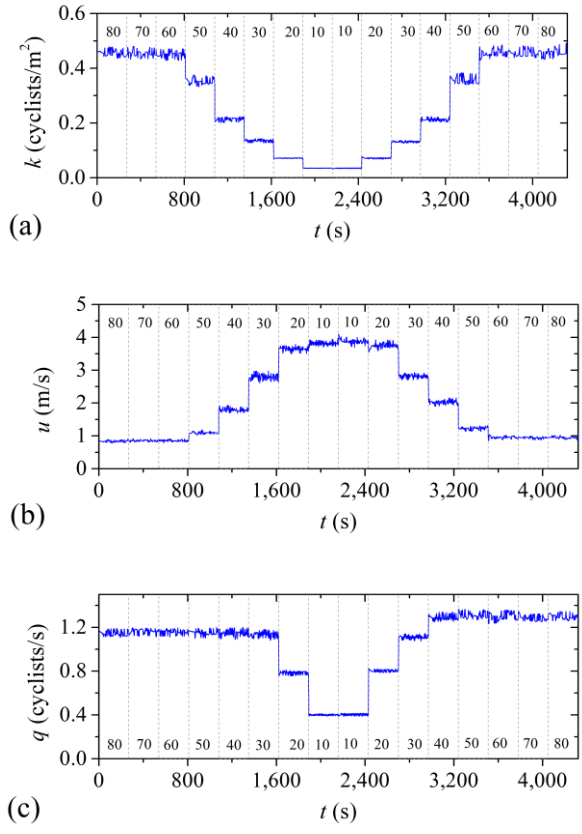

Figure 9. Evolution of (a) k, (b) u, and (c) q in Runs 1 and 2 with the 1.5 m bottleneck.

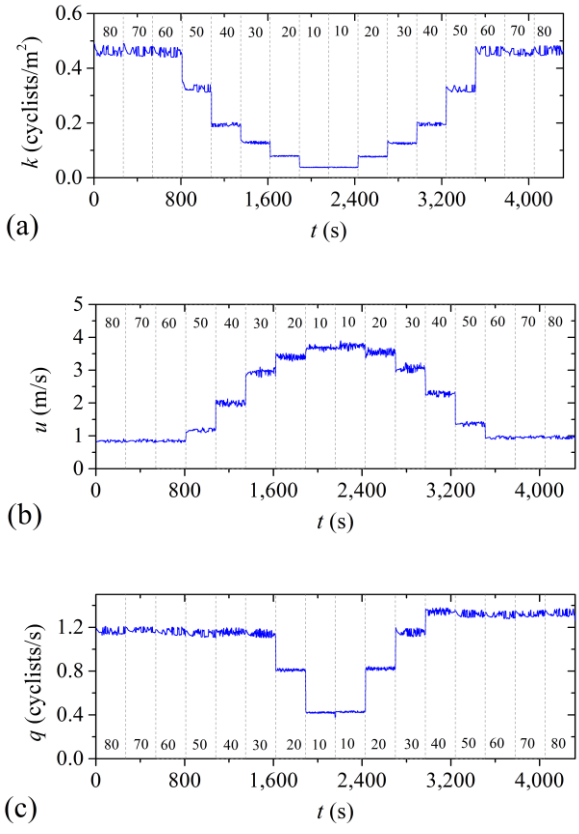

Figure 10. Evolution of (a) k, (b) u, and (c) q in Runs 3 and 4 with the 1.5 m bottleneck.

In Run 2, the number of cyclists increased from 10 to 80. As more cyclists were allowed to enter the track, k increased in a stepwise manner, indicating that the cyclists in the upstream subarea were

becoming more closely spaced. The increased interactions between cyclists led to a stepwise decrease in u. As the number of cyclists increased from 10 to 40, the effect of increase in k outweighed the effect of decrease in u, leading to a stepwise increase in q. When the number of cyclists increased from 40 to 60, k continued to increase and u continued to decrease; however, the two effects counterbalanced each other, resulting in a bottleneck capacity of approximately 1.3 cyclists/s. This observation indicated that the bottleneck was activated. When the number of cyclists increased from 60 to 80, k, u and q remained largely constant, indicating that the upstream subarea was fully occupied by the bicycle queue. Similar to the results presented in the previous subsection, the bottleneck capacity for the cyclist loading process was higher than that of the cyclist unloading process.

Figure 10 depicts the evolutions of k, u, and q over time for Runs 3 and 4. The patterns were similar to those in Figure 9, which indicated that the observed pattern and capacity drop were not influenced by the ordering and individual characteristics of cyclists.

6.3. Relationship between the flow and density

To investigate the evolution of flow against density, the high-resolution q was plotted against k. As demonstrated in Figure 11, the bottleneck capacity for the cyclist loading process was greater than that for the cyclist unloading process once the bottleneck was activated, indicating the occurrence of capacity drops. Moreover, the evolution paths of the flow against density for the cyclist loading and unloading processes were different, suggestive of hysteresis. This observation suggested that the current bicycle state is influenced by previous states, and thus, the bottleneck capacity (or bicycle state) is path-

dependent. These results pose an intriguing research question regarding the potential factors contributing to the capacity drop and hysteresis phenomena.

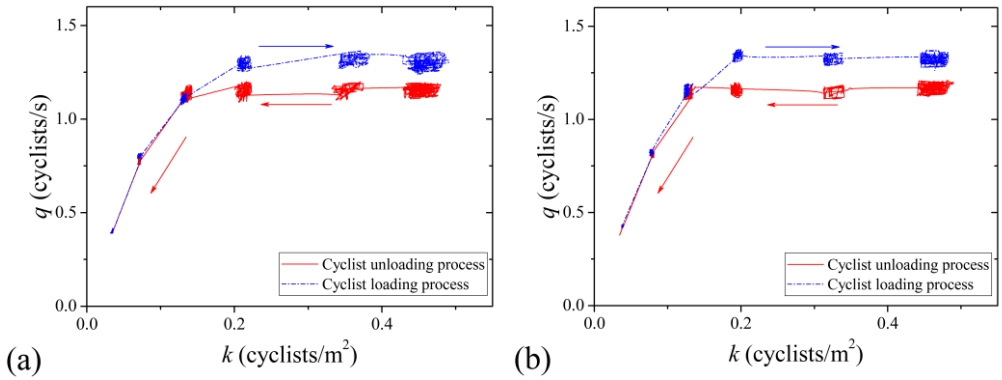

Figure 11. Relationship between q and k in (a) Runs 1 and 2 and (b) Runs 3 and 4.

6.4. Cause of capacity drop

According to the analyses, the bottleneck capacities for the cyclist loading and unloading processes were different once the bottleneck was activated. Since q is the product of w_c, u, and k, in theory, the capacity drop could be caused by (1) differences in the speeds, (2) differences in the densities, or (3) differences in both between the cyclist loading and unloading processes for a given cycling demand under which the bottleneck was activated. To test this hypothesis, statistical tests were performed to determine (1) if the densities and (2) speeds of the two processes were statistically different after bottleneck activations. The null hypotheses were defined as follows: For the cyclist loading and unloading processes, (1) there was no significant difference between the density means, and (2) there was no significant difference between the speed means. Table 2 summarizes the statistics for the t-tests. Using a significance level of 0.05, the p-value for testing the difference in the densities for each given cycling demand was greater than 0.05. Thus, there was insufficient statistical evidence to support the rejection of the null hypothesis. Conversely, the p-value for testing the difference in the speeds for each

given cycling demand was smaller than 0.05. This result indicated that there was sufficient statistical evidence to reject the null hypothesis, and thus, the observed difference in speeds between the two processes was statistically significant. Thus, the capacity drop was attributable to the difference in speeds in the two processes.

Table 2. Results of *t*-tests for the differences in the densities and speeds at different cycling demands

Cycling demand	*p*-value for testing the difference in densities	*p*-value for testing the difference in speeds
80	0.64	0.00
70	0.51	0.00
60	0.58	0.00
50	0.46	0.00
40	0.12	0.00

Figure 12 depicts the relationship between the average upstream space-mean speed and average upstream density in (a) Runs 1 and 2 and (b) Runs 3 and 4 with a 1.5 m bottleneck. The empirical results indicated that for a given average upstream density, the average upstream space-mean speed of the cyclist loading process was higher than that of the cyclist unloading process, consistent with the results of the statistical tests described above.

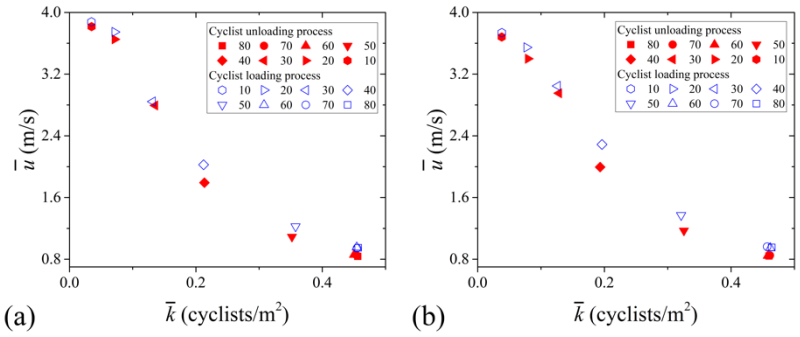

Figure 12. Average upstream space-mean speed and average upstream density in (a) Runs 1 and 2 and (b) Runs 3 and 4 with the 1.5 m bottleneck.

6.5. Behavioral inertia

The observed capacity drop and hysteresis phenomena could be attributed to the statistically significant differences in speeds between the cyclist loading and unloading processes. These outcomes suggest that the current bicycle state is influenced by previous states, and thus, behavioral inertia (Train, 2003) could possibly be the governing cycling behavior. Behavioral inertia, similar to the inertia described in Newton's first law, refers to individuals' tendency to remain in their current behavioral states as they lack motivation to change their behavior. Thus, it could be hypothesized that in the cyclist loading process, cyclists tend to consistently travel at a higher speed and maintain their speed even as they gradually become more closely spaced and interact more. To test this hypothesis, another series of single-cyclist experiments were conducted. The objective was to examine the potential existence of behavioral inertia in cycling, specifically, the tendency of cyclists to maintain their current speed levels even when changes in speed were required.

An oval-shaped cycle track with a radius of 6 m for the semi-circular segments, as shown in Figure 1, was used for the experiments. Ten undergraduate students, seven male and three female, participated in the experiment. To test the behavioral inertia, four speed levels were defined: maximum speed v_0, high speed $0.75v_0$, moderate speed $0.5v_0$, and low speed $0.25v_0$, where v_0 is the participant-specific free-flow speed. First, the bicycle was equipped with a speedometer, and the participants practiced maintaining their cycling speeds at the four defined levels. Before the start of the experiments, the speedometer was removed from the bicycle. Two experimental runs were performed, corresponding to the acceleration and deceleration branches. In the acceleration branch, each participant was instructed

to gradually increase their cycling speed from the low speed level to the maximum speed level. In the deceleration branch, each participant was instructed to gradually decrease their cycling speed from the maximum speed level to the low speed level. At each of the four speed levels, the participant cycled four laps around the track.

Figure 13 displays the average cycling speeds of the participants at different instructed speed levels for the acceleration and deceleration branches. At each instructed speed level, the average cycling speed of the participants in the deceleration branch was consistently higher than that in the acceleration branch. These results suggested that cyclists tended to maintain their previous speeds even when instructed to change speed, consistent with the notion of behavioral inertia. This behavioral inertia likely originated from the human perception of speed. The human perception of speed is typically relative: When a person traveling at a speed of 100 km/h on a highway transitions to a speed of 50 km/h on an urban road, they would perceive 50 km/h to be slower than usual due to their most recent memory. Therefore, in the experiments, the cyclists who were initially traveling at high speeds and were forced to decelerate likely perceived the required speed based on their original speed, leading to them continue at higher speeds. Thus, behavioral inertia could be a plausible explanation for the observed results.

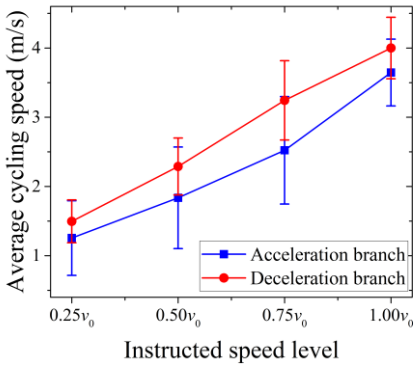

Figure 13. Average cycling speeds of participants at different instructed speed levels.

To maintain higher speeds for the cyclist loading process under the same density, cyclists would need to aggressively maintain a higher overtaking rate. The overtaking rate is defined as the number of overtaking maneuvers performed in the upstream subarea over each stage in an experimental run. The value is determined by comparing the sequences of cyclists entering and exiting A. For instance, if the $(i+1)^{th}$ cyclist enters the upstream subarea after the i^{th} cyclist but exits before the i^{th} cyclist, the $(i+1)^{th}$ cyclist must have overtaken the i^{th} cyclist, indicating one overtaking event. Figure 14 illustrates the overtaking rates in the upstream subarea against the average upstream density in (a) Runs 1 and 2 and (b) Runs 3 and 4. In the cyclist unloading process, few cyclists overtook others owing to the limited space. As the average upstream density decreased, despite some fluctuation and enhancement, the overtaking rate remained low. In contrast, in the cyclist loading process, the overtaking rate was initially high because space was available. Interestingly, the overtaking rate remained high even at a higher average upstream density. Despite some fluctuations, the overtaking rates of bicycle flow for the cyclist loading process were always higher than those for the cyclist unloading process. These findings support the hypothesis that the cyclists exhibited behavioral inertia, that is, their behavior was affected by their previous states and thus exhibited temporal dependence. Behavioral inertia can also explain how cyclists maintained higher speeds in the cyclist loading process than those in the cyclist unloading process.

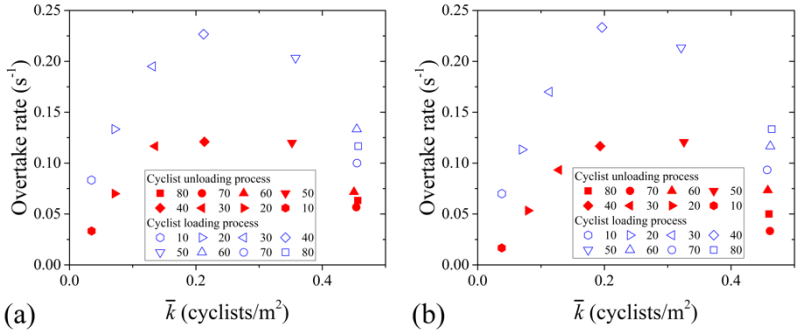

Figure 14. Overtaking rates in the upstream subarea against the average upstream density in (a) Runs 1 and 2 and (b) Runs 3 and 4 with the 1.5 m bottleneck.

7. Conclusions

The bicycle flow dynamics at bottlenecks were investigated through a series of cycling experiments with varying cycling demands. Specifically, the cyclist unloading and loading processes were examined. The experiments were conducted on a classic oval-shaped cycle track with a width of 3 m. The track dimensions were carefully selected to ensure that the radii of the semi-circular segments were large enough to minimize the impact on speed profiles due to turning and the straight segments were long enough to allow cyclists to return to their desired speed before crossing the bottleneck.

Detailed cyclist trajectory data were extracted from the recorded footage. The upstream bicycle speed, density, and flow were acquired on a per-second basis; and the average upstream bicycle speed, density, and flow were acquired on a per-stage basis. Analysis of the data revealed that upon bottleneck activation, bottleneck capacities remained nearly constant. However, the bottleneck capacities for the cyclist unloading and loading processes were different, even though the same physical system was considered. These observations indicated the presence of a capacity drop for varying cycling demands. Moreover, the evolutions of the upstream bicycle speed, density, and flow were examined to investigate the bicycle flow dynamics at bottlenecks. In addition to the capacity drop, hysteresis was observed,

implying that the current bicycle state was influenced by the previous states and that the evolution of bicycle flow at bottlenecks was path-dependent. Statistical analyses showed that the capacity drop and hysteresis phenomena were attributable to the significant differences in speeds between the two processes. These patterns could be explained by the cyclists' behavioral inertia, i.e., their tendency to maintain their previous riding behavior. Further examination revealed that the sustained higher speeds in the cyclist loading process were achieved through higher overtaking rates than those in the unloading process. This study enhances our comprehension of bicycle flow dynamics at bottlenecks while providing valuable insights for transportation planning professionals in the design of new facilities and management of current networks.

Acknowledgments

This work was supported by the National Natural Science Foundation of China (Grant 72288101, 71931002); Guangdong-Hong Kong-Macau Joint Laboratory Program of the 2020 Guangdong New Innovative Strategic Research Fund, Guangdong Science and Technology Department (Project 2020B1212030009); and Fundamental Research Funds for the Central Universities (JZ2023YQTD0073). The fourth author was also supported by the Francis S Y Bong Professorship in Engineering.

References

Barrero GA, Rodriguez-Valencia A (2022) Asking the user: a perceptional approach for bicycle infrastructure design. *Int. J. Sustain. Transp.*, 16: 246-257.

Beura SK, Kumar NK, Bhuyan PK (2017) Level of service for bicycle through movement at signalized intersections operating under heterogeneous traffic flow conditions. *Transp. Dev. Econ.* 3: 21.

Boltes M, Seyfried A, Steffen B, Schadschneider A (2010) Automatic extraction of pedestrian trajectories from video recordings. *Pedestrian and Evacuation Dynamics 2008*. Springer, 43-54.

Botma H, Papendrecht H (1991) Traffic operation of bicycle traffic. *Transp. Res. Rec.*, 1320: 65-72.

Gavriilidou A, Wierbos MJ, Daamen W, YY, Knoop VL, Hoogendoorn SP (2019) Large-scale bicycle flow experiment: setup and implementation. *Transp. Res. Rec.* 2673: 709-719.

Gould G, Karner A (2009) Modeling bicycle facility operation cellular automaton approach. *Transp. Res. Rec.* 2140: 157-164.

Guo N, Jiang R, Wong SC, Hao QY, Xue SQ, Hu MB (2021) Bicycle flow dynamics on wide roads: Experiments and simulation. *Transp. Res. C* 125: 103012.

Guo N, Jiang R, Wong SC, Hao QY, Xue SQ, Xia Y, Wu CY (2020) Modeling the interaction of pedestrians and cyclists in mixed flow conditions in uni- and bidirectional flows on a shared pedestrian-cycle road. *Transp. Res. B* 139: 259-284.

Homburger WS (1976) Capacity of bus routes and of pedestrian and bicycle facilities. Institute of Transportation Studies, University of California at Berkeley, Berkeley, CA.

Hoogendoorn SP, Daamen W (2005) Pedestrian behavior at bottlenecks. *Transp. Sci.* 39: 147-159.

Jia B, Li XG, Jiang R, Gao ZY (2007) Multi-value cellular automata model for mixed bicycle flow. *Eur. Phys. J. B* 56: 247-252.

Jiang R, Hu MB, Wu QS, Song WG (2017) Traffic dynamics of bicycle flow: experiment and modeling. *Transp. Sci.* 51: 998-1008.

Jiang R, Jia B, Wu QS (2004) Stochastic multi-value cellular automata models for bicycle flow. *J. Phys. A* 37: 2063-2072.

Jin HY, Jin WL (2015) Control of a lane-drop bottleneck through variable speed limits. *Transp. Res. C* 58: 568-584.

Jin S, Qu XB, Xu C, Ma DF, Wang DH (2015) An improved multi-value cellular automata model for heterogeneous bicycle traffic flow. *Phys. Lett. A* 379: 2409-2416.

Liang X, Mao B, Xu Q (2012) Psychological-physical force model for bicycle dynamics. *J. Transp. Sys. Eng. Inf. Technol.* 12: 91-97.

Mai X, Lv W, Wei XG, Song WG, Jiang R (2012) Analyzing the characteristics of unidirectional bicycle movement around a track based on digital image processing. *9th Asia-Oceania Symposium on Fire Science and Technology*, Oct 17-20, 2012, Hefei, China.

Meng Q, Weng JX (2011) An improved cellular automata model for heterogeneous work zone traffic. *Transp. Res. C* 19: 1263-1275.

Mohammed H, Bigazzi AY, Sayed T (2019) Characterization of bicycle following and overtaking maneuvers on cycling paths. *Transp. Res. C* 98: 139-151.

Navin FPD (1994) Bicycle traffic flow characteristics: experimental results and comparisons. *ITE J.* 64: 31-36.

Ni D (2021) Field theory for some traffic phenomena and fundamental diagram. *Transp. Res. Rec.* 2675: 1195-1208.

Olmos LE, Tadeo MS, Vlachogiannis D, Alhasoun F, Alegre XE, Ochoa C, Targa F, González MC (2020) A data science framework for planning the growth of bicycle infrastructures. *Transp. Res. C* 115: 102640.

Paulsen M, Rasmussen TK, Nielsen OA (2019) Fast or forced to follow: A speed heterogeneous approach to congested multi-lane bicycle traffic simulation. *Transp. Res. B* 105: 315-327.

Raksuntorn W, Khan SI (2003) Saturation flow rate, start-up lost time, and capacity for bicycles at signalized intersections. *Transp. Res. Rec.* 1852: 105-113.

Ren G, Jiang H, Chen JX, Huang ZF, Lu LL (2016) Heterogeneous cellular automata model for straight-through bicycle traffic at signalized intersection. *Physica A* 451: 70-83.

Saberi M, Mahmassani H (2013) Hysteresis and capacity drop phenomena in freeway networks: empirical characterization and interpretation. *Transp. Res. Rec.*, 2391(1), 44–55.

Seyfried A, Passon O, Steffen B, Boltes M, Rupprecht T, Klingsch W (2009) New insights into pedestrian flow through bottlenecks. *Transp. Sci.* 43: 395-406.

Train KE (2003) Discrete choice models with simulation. Cambridge University Press, Cambridge, UK.

Wierbos MJ, Knoop VL, Hänseler FS, Hoogendoorn SP (2019) Capacity, capacity drop, and relation of capacity to the path width in bicycle traffic. *Transp. Res. Rec.* 2673: 693-702.

Wierbos MJ (2021) Macroscopic characteristics of bicycle traffic flow a bird's-eye view of cycling. Delft University of Technology.

Wierbos MJ, Knoop VL, Bertini RL, Hoogendoorn SP (2021) Influencing the queue configuration to increase bicycle jam density and discharge rate: an experimental study on a single path. *Transp. Res. C* 122: 102884.

Xue SQ, Jia B, Jiang R, Li XG, Shan JJ (2017) An improved Burgers cellular automaton model for bicycle flow. *Physica A* 487: 164-177.

Zhang J, Mehner W, Holl S, Boltes M, Andresen E, Schadschneider A, Seyfried A (2014) Universal flow-density relation of single-file bicycle, pedestrian and car motion. *Phys. Lett. A* 378: 3274-3277.

Appendix A. Validation of PeTrack by Tracker

PeTrack is a widely used software for the automatic extraction of pedestrian trajectories. This software considers lens distortion and perspective view to project the marked heads of pedestrians onto the ground, thereby obtaining their coordinates and trajectories. In general, pedestrians and cyclists have similar heights and differ mainly in terms of their movement speeds, which does not affect the fundamental functioning of the software. Thus, PeTrack is considered suitable for extracting cyclist trajectories.

The Tracker software was used to validate the accuracy of the cyclist trajectories extracted using PeTrack. To this end, the footage of three randomly selected cyclists travelling along the 25-m-long straight segment of the cycle track was examined. The trajectories of the three cyclists extracted by PeTrack and Tracker are shown in Figure A. The *X*-axis represents the length of the straight segment, and the *Y*-axis represents the width of the straight segment. The trajectories extracted by both software are nearly identical, which indicates that the accuracy and performance of the two software are consistent and satisfactory.

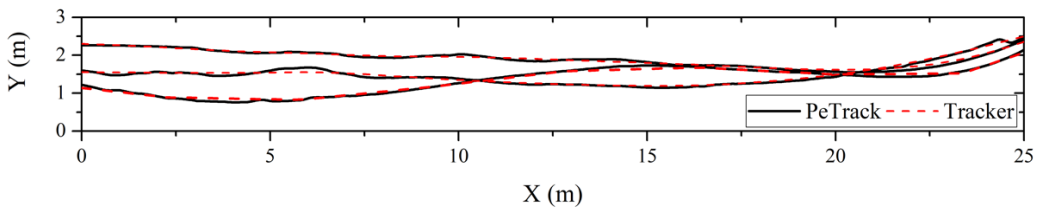

Figure A. Comparison of trajectories extracted by PeTrack and Tracker